Supplementary Information for

Mantle-driven plate convergence due to slab detachment

Yangming Wu[1*], Manuele Faccenda[2], Jie Liao[3,4], Jianke Fan[5], Feng Guo[6] & Zhongping Lai[1]

[1]*Institute of Marine Sciences, Guangdong Provincial Key Laboratory of Marine Disaster Prediction and Prevention, Shantou University, Shantou, China.*

[2]*Dipartimento di Geoscienze, Università di Padova, via Gradenigo 6, Padova, Italy.*

[3]*School of Earth Sciences and Engineering, Sun Yat-Sen University, Guangzhou, China.*

[4]*Southern Marine Science and Engineering Guangdong Laboratory (Zhuhai), Zhuhai, China.*

[5]*Key Laboratory of Ocean Observation and Forecasting, Key Laboratory of Marine Geology and Environment, Institute of Oceanology, Chinese Academy of Sciences, Qingdao, China.*

[6]*College of Resources and Environment, Yangtze University, Wuhan, China*

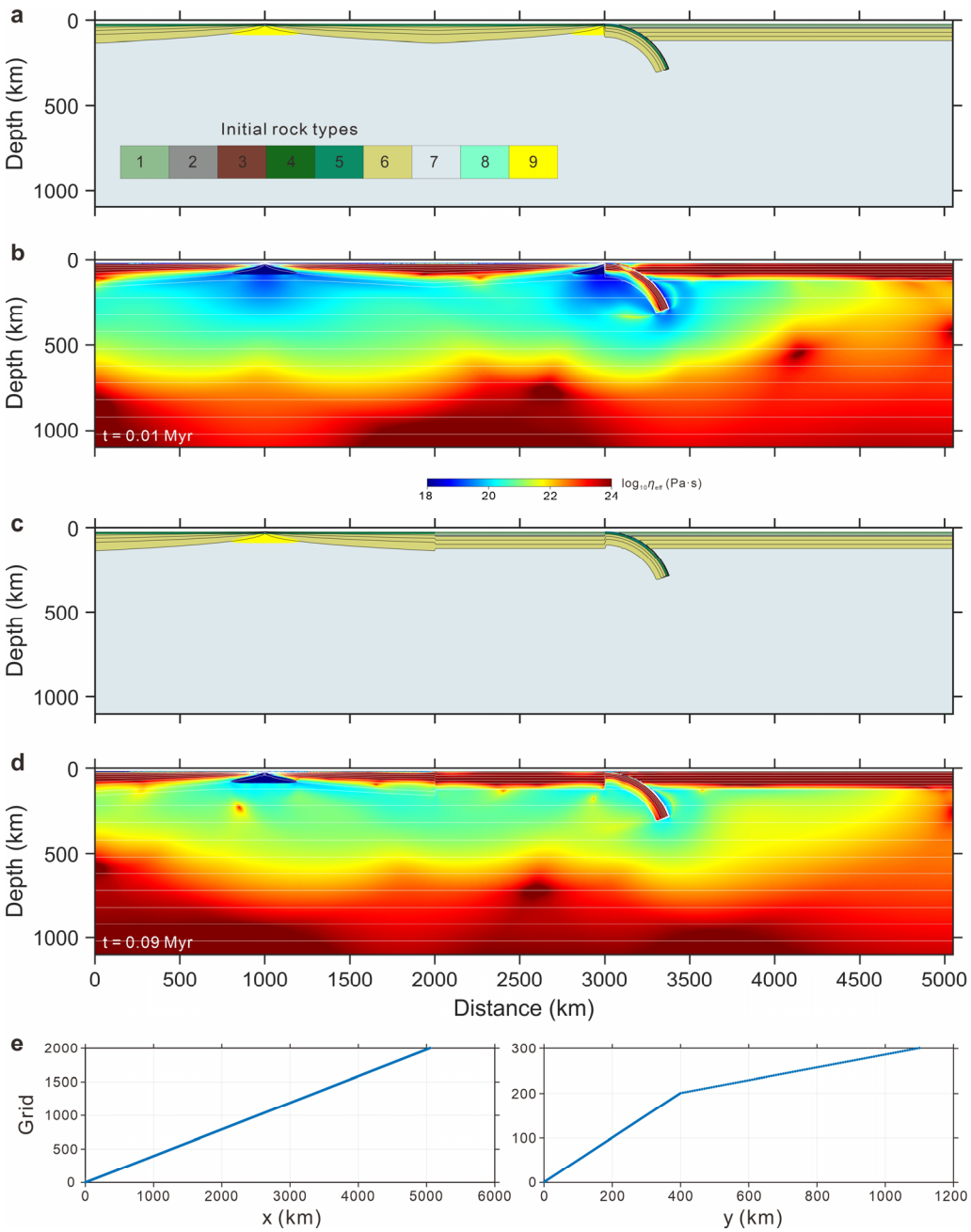
*Correspondence to: Yangming Wu, yangmingwu@stu.edu.cn

This file includes:

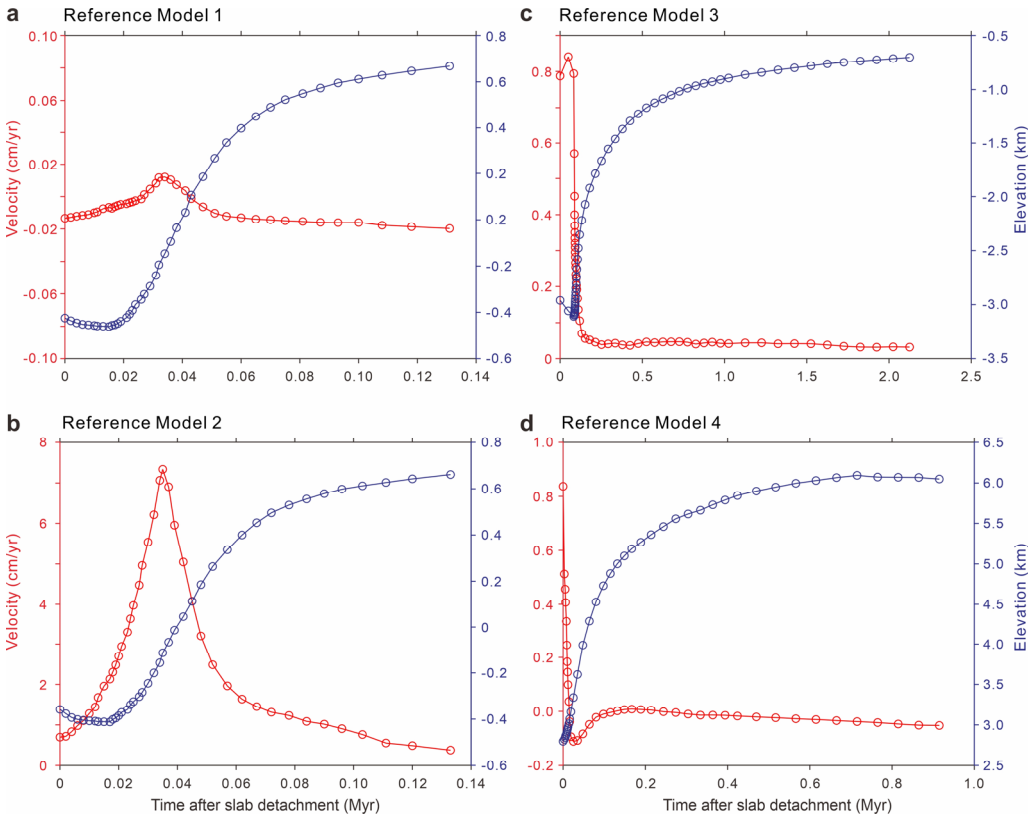
1. Supplementary Figures S1-S7

2. Supplementary Table 1

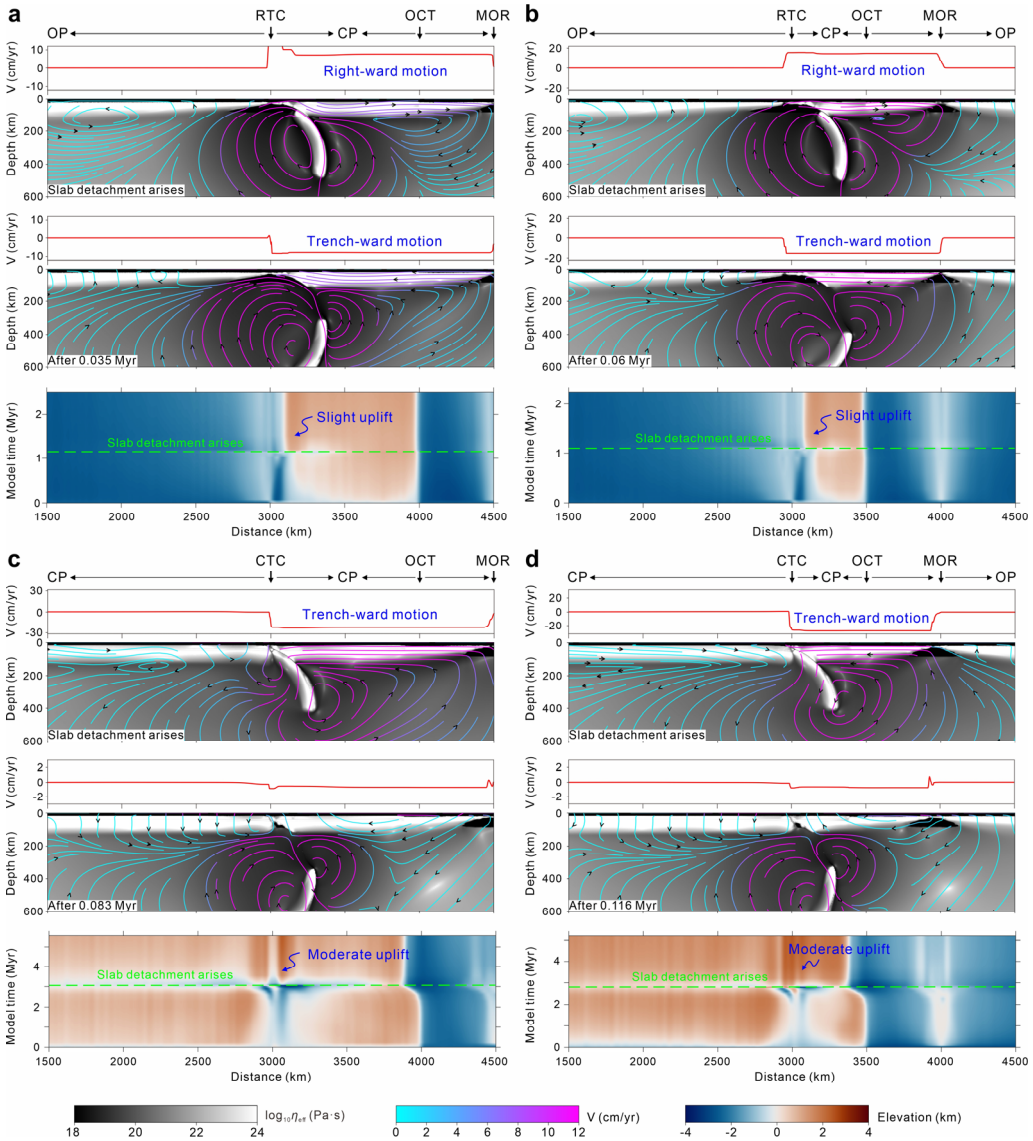
3. Supplementary References



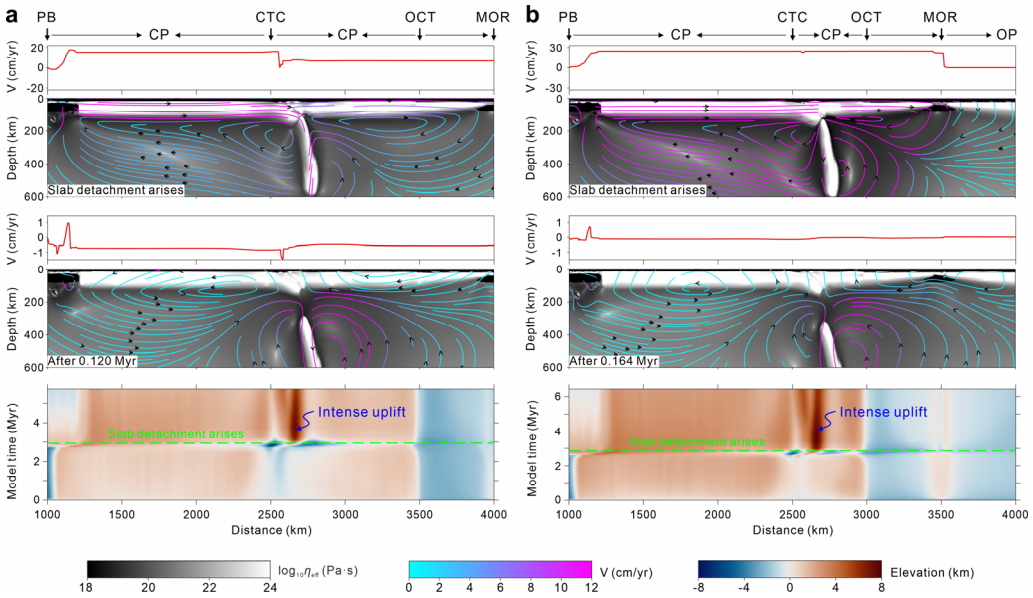
Supplementary Fig. 1 Configuration of the initial reference model. a The composition field of the reference ridge-trench collision model. b The initial model evolution of viscosity field of a. c The composition field of the reference continent-trench collision. d The initial model evolution of viscosity field of c. The black lines in a and c demonstrate the isotherms of 400, 700, 1000, and 1300 ℃. The white lines in b and d denote the isotherms from 100 to 1300 ℃ with an increment of 300 ℃ in the lithosphere and from 1350 to 1750 ℃ with an increment of 50 ℃. e Model size and spatial resolution in x and y direction. A color legend is shown below, including initial and newly formed rocks types: 1-upper continental crust; 2-lower continental crust; 3-sediment; 4-oceanic basaltic crust; 5-oceanic gabbroic crust; 6-lithospheric mantle; 7-asthenosheric mantle; 8-water; 9-molten mantle.



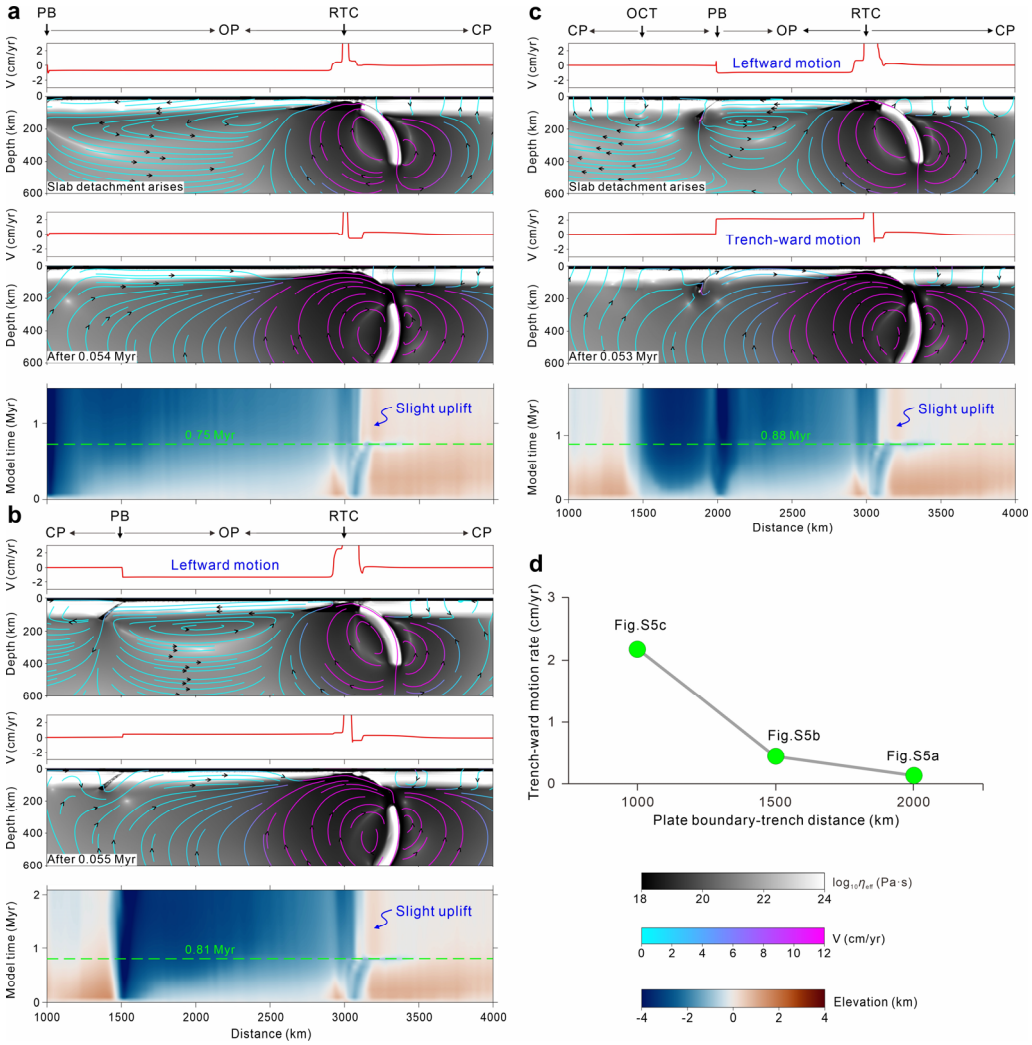
Supplementary Fig. 2 Evolution of the motion rate of the subducting plate and the topography of the suture zone after slab detachment in the four different reference models. **a** Ridge-trench collision without plate boundary weakness on the subducting plate. **b** Ridge-trench collision with mid-ocean ridge on the subducting plate. **c** Continental-trench collision without plate boundary weakness on the subducting plate. **d** Continent-trench collision with mid-ocean ridge on the subducting plate. The red circles indicate the motion rate of the subducting plate, calculated from the mean value in the range y = 28 km depth (i.e., 8 km below the initial surface) and x = 1500-2500 km. The blue circles indicate the elevation of the suture zone, calculated from the maximum value at x = 3100-3200 km in the suture zone. The horizontal axis denotes the time at which relative slab detachment arises.



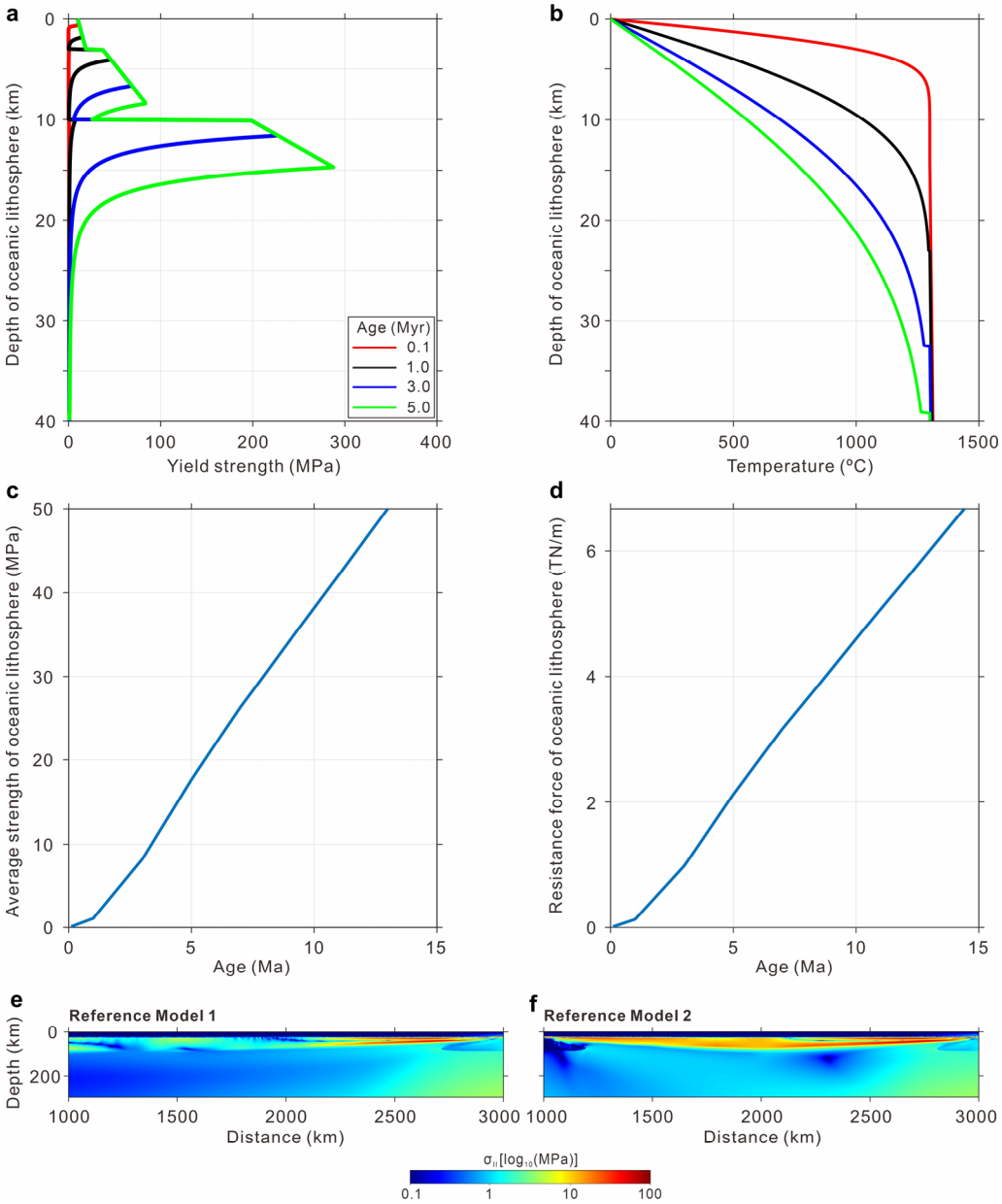
Supplementary Fig. 3 Test the effect of a mid-ocean ridge prescribed on the overriding plate. **a** and **b** Ridge-trench collision model. The distance from the mid-ocean ridge to the trench is 1500 km in **a** and 1000 km in **b**. **c** and **d** Continent-trench collision model. The distance from the mid-ocean ridge to the trench is 1500 km in **c** and 1000 km in **d**. The velocity profile on the top of each panel is obtained at the depth of y = 28 km in the model. Velocity is positive to the right and negative to the left. The upper and lower model snapshots display the onset of slab detachment and subsequent vigorous mantle flows, respectively. The time of the lower snapshot is relative to the upper snapshot. The bottom of each panel shows the topographic evolution over model time, with the green dashed line indicating the onset time of slab detachment. Color palettes at the figure base represent viscosity, mantle flow velocity, and elevation from left to right.



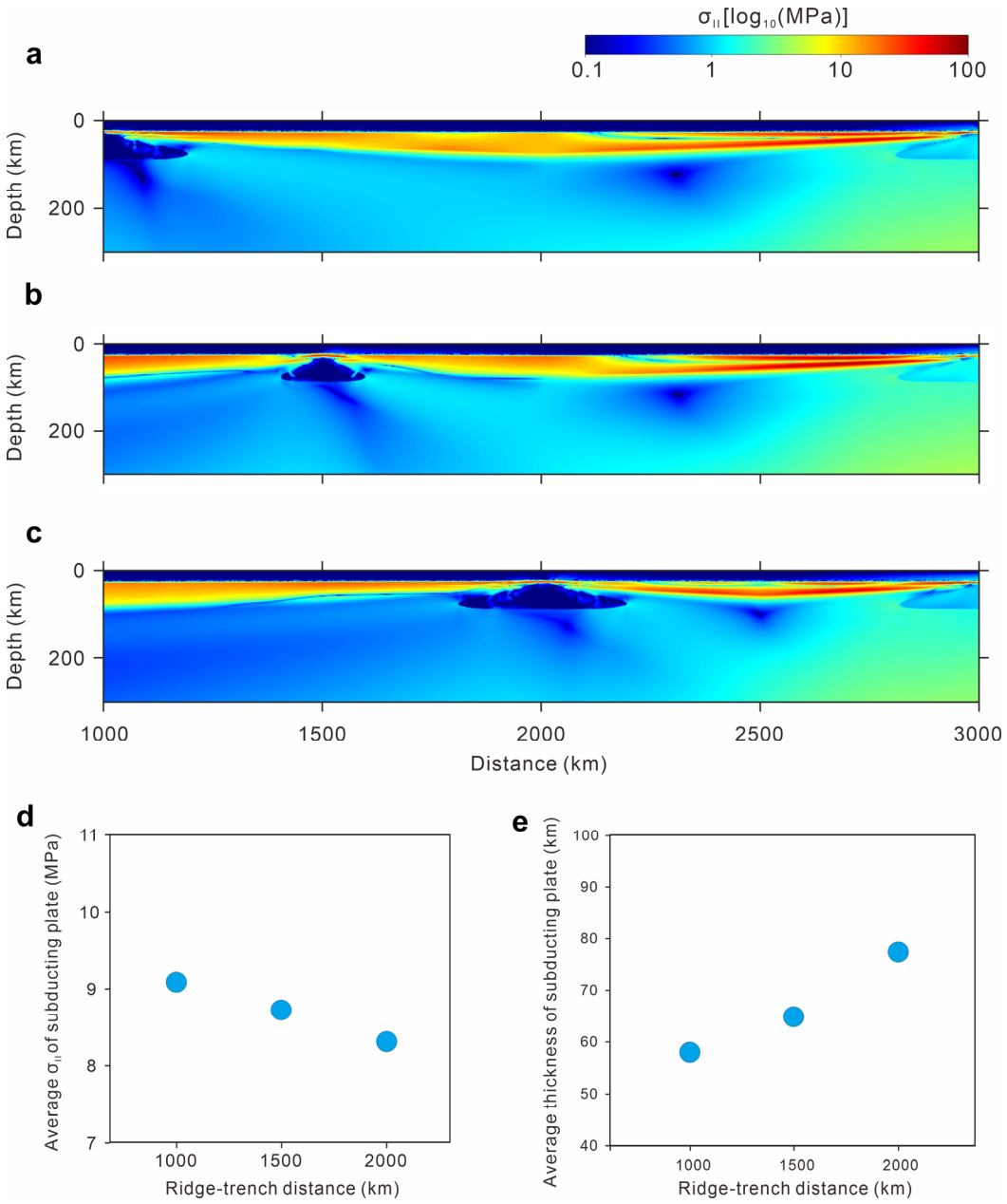
Supplementary Fig. 4 Test the effect of plate boundary both on the trailing and overriding plates. The plate boundary on the trailing plate is 1500 km to the trench. **a** The distance from the mid-ocean ridge to the trench is 1500 km. **b** The distance from the mid-ocean ridge to the trench is 1000 km. Velocity profiles, model snapshots, topography evolution plots, and color palettes follow the conventions established in Fig. S3.



Supplementary Fig. 5 Test the effect of plate size in the case of a weak plate boundary prescribed on the trailing plate. The distance from the plate boundary to the trench is 2000 km in **a**, 1500 km in **b**, and 1000 km in **c.** Velocity profiles, model snapshots, topography evolution plots, and color palettes follow the conventions established in Fig. S3.



Supplementary Fig. 6 Ridge axis strength with different ages. **a** Yield envelope profiles of the ridge axis with different ages subjected to extensional deformation (strain rate = $10^{-14}s^{-1}$). **b** Temperature profiles of the ridge axis with different ages. **c** Average strength of ridge axis at different ages. **d** Resistance force of ridge axis at different ages. The thickness and temperature structure of the ridge axis were calculated by the half-space cooling model[1]. **e** and **f** show the second invariant of the deviatoric stress tensor ($\sigma_{II} = \sqrt{\sigma_{xx}^2 + \sigma_{xy}^2}$) of the reference model 1 and 2, respectively.



Supplementary Fig. 7 Effect of plate size on the second invariant of the deviatoric stress tensor (σ_{II}) of the subducting plate during slab detachment. **a-c** Ridge-trench distance is 2000, 1500, and 1000 km, respectively. **d** Average second invariant of the deviatoric stress tensor ($\sigma_{\mathrm{II}}^{average}$) of the subducting plate versus ridge-trench distance. **e** Average thickness ($h^{average}$) of subducting plate versus ridge-trench distance. The accelerated speed (Δv) of the subducting plate can be simply expressed by $\Delta v = (\sigma_{\mathrm{II}}^{average} L)/(\rho h^{average} L)$, where ρ denotes density, L denotes the length of the subducting plate. Thus, the accelerated speed is proportional to stress and inversely proportional to the thickness of the subducting plate.

Supplementary Table 1 Physical properties of rocks used in numerical experiments

Material	**ρ_0[1,2], (kg/m^3)**	**Thermal conductivity k[3,4], (W/m/K at T_K, P_{MPa})**	**Flow law[5]**
Sediment	2600	0.64+807/(T+77) × exp(0.00004P)	wet quartzite, A=1.97×10^{17} Pa^{n}s, n=2.3, E=154 kJ/mol, V=8 J/mol/MPa, σ_{cr}=3×10^4 Pa, C=1 MPa, μ=0
Upper oceanic crust (basalt)	3000	1.18+474/(T+77)× exp(0.00004P)	Plagioclase An$_{75}$, A=4.8×10^{22} Pa^{n}s, n=2.3, E=238 kJ/mol, V=8 J/mol/MPa, σ_{cr}=3×10^4 Pa, C_0=10 MPa, C_1=1 MPa, μ_0=0.1, μ_1=0.05
Lower oceanic crust (gabbro)			Plagioclase An$_{75}$, A=4.8×10^{22} Pa^{n}s, n=3.2, E=238 kJ/mol, V=8 J/mol/MPa, σ_{cr}=3×10^4 Pa, C_0=10 MPa, C_1=1 MPa, μ_0=0.3, μ_1=0.15
Upper continental crust	2750	0.64+807/(T+77) × exp(0.00004P)	wet quartzite, A=1.97×10^{17} Pa^{n}s, n=2.3, E=154 kJ/mol, V=8 J/mol/MPa, σ_{cr}=3×10^4 Pa, C=1 MPa, μ_0=0.2, μ_1=0.1
Lower continental crust	2850	1.18+474/(T+77) × exp(0.00004P)	felsic granulite, A=4.97×10^{20} Pa^{n}s, n=3.1, E=532 kJ/mol, V=10 J/mol/MPa, σ_{cr}=3×10^4 Pa, C=1 MPa, μ_0=0.3, μ_1=0.15
Lithosphere – Asthenosphere mantle	3300	0.73+1293/(T+77)× exp(0.00004P)	dry olivine, A=3.98×10^{16} Pa^{n}s, n=3.5, E=532 kJ/mol, V=8 J/mol/MPa, σ_{cr}=3×10^4 Pa, C_0=20 MPa, C_1=10 MPa, μ_0=0.6, μ_1=0.4
Weak zone			wet olivine, A=5.01×10^{20} Pa^{n}s, n=4.0, E=470 kJ/mol, V=8 J/mol/MPa, σ_{cr}=3×10^7 Pa, C=1 MPa, μ_0=0.6, μ_1=0.4

Supplementary References

1. Turcotte DL, Schubert G. Geodynamics. Cambridge University Press (2002).

2. Bittner D, Schmeling H. Numerical Modelling of Melting Processes and Induced Diapirism In the Lower Crust. Geophysical Journal International 123, 59-70 (1995).

3. Clauser C, Huenges E. Thermal conductivity of rocks and minerals. Rock physics and phase relations: a handbook of physical constants 3, 105-126 (1995).

4. Hofmeister AM. Mantle values of thermal conductivity and the geotherm from phonon lifetimes. Science 283, 1699-1706 (1999).

5. Ranalli G. Rheology of the Earth. Springer Science & Business Media (1995).